A Novel Tunable Fiber-optic Microwave Filter using Fiber Modes in DCF

연세대학교 대학원

전기전자 공학과

이 광 현

A Novel Tunable Fiber-optic Microwave Filter using Fiber Modes in DCF

지도 최 우 영 교수

이 논문을 석사 학위논문으로 제출함

2002 년 12 월 일

연세대학교 대학원

전기·전자공학과

이 광 현

이광현의 석사 학위논문을 인준함

심사위원_____인

심사위원_____인

심사위원_____인

연세대학교 대학원

2002년 12월 일

A Novel Tunable Fiber-optic Microwave Filter using Fiber Modes in DCF

By

Kwang-Hyun Lee

Submitted to the Department of Electrical and Electronic Engineering
in partial fulfillment of the requirements for the Degree
Master of Science

at the

Department of Electrical and Electronic Engineering
The Graduate School
YONSEI University
Seoul, KOREA

December 2002

Index

Figure Index

Table Index

Abstract

A Novel Tunable Fiber-optic Microwave Filter using Fiber Modes in DCF

Lee, Kwang-Hyun
Dept. of Electrical and Electronic Eng.
The Graduate School
Yonsei University

In this thesis, a novel fiber-optic microwave filter composed of one optical source and one multimode dispersion compensation fiber (DCF) is proposed and demonstrated. The proposed filter uses the velocity difference among guided modes in multimode DCF as the basic mechanism for optical delay lines and the power coupling ratio into these modes is controlled by the hollow optical fiber (HOF). In this filter, the tap number is determined by the mode number in DCF, thus multi-taps can be achieved with one multimode DCF. In addition, the free spectral range (FSR) can be easily controlled by tuning the incident light wavelength.

To find the filter characteristic, the time delay is calculated numerically from Maxwell's equations and the analytic form of frequency response is

derived. In this thesis, the two-tap filter response having 1GHz FSR is shown. The tuning characteristic of FSR is shown clearly with the tuning rate of 0.285ns/km·nm. In addition, the notch rejection is more than 20dB for wavelengths covered in the experiment.

Keywords: dispersion compensation fiber, fiber-optic filter, microwave, hollow optical fiber, optical time delay, tapped delay line filter

Ⅰ. Introduction

Generally, the optical fiber has been used in optical communications or optical networks as a transmission medium due to low loss and low dispersion. However, it can also be used as a delay medium for broadband signal processing. It is firstly proposed by Wilner and vanden Heuvel [1]. The use of optical fiber as a delay medium is very attractive because of three reasons: low loss, linearity (Dynamic range) [2], and compact size.

The signal loss, or attenuation, in optical fibers is induced from a number of wavelength dependent mechanisms such as Rayleigh scattering and infrared absorption. Below the wavelength of about 1.6μm, Rayleigh scattering is the dominant loss mechanism, but this effect is reduced to below 0.01dB/km at the wavelength longer than 3μm. At longer wavelength, the most dominant loss is infrared absorption losses. If both the absorption losses and Rayleigh scattering loss is combined, the optical loss profile having minimum (0.2dB/km) near 1.5μm is obtained. Although the optical loss is dependent of the source wavelength, the propagation loss, at fixed source wavelength, of the fiber is independent of the modulating signal frequency. It is a very important and attractive characteristic different from other delay media in relation to broadband signal processing.

The linearity, or dynamic range, of an optical fiber is determined by the

quantum noise of photo diodes and by nonlinear loss induced within optical fiber [3]. All receivers require the minimum received power, defined noise equivalent power (NEP), for the envelope detection. The NEP can be expressed by

$$NEP = 2hvB \tag{1.1}$$

where h is Plank's constant, v is the spectral frequency of the signal, and B is the bandwidth. The NEP is the lower limit of dynamic range. The upper limit of dynamic range is set by stimulated Raman scattering (SRS). The critical input power $\boldsymbol{P}_{\text{crit}}$ above which SRS effect can not be negligible is given by

$$P_{crit} \approx 21\frac{A}{\gamma_0 L} \tag{1.2}$$

where A is cross sectional area of the fiber core, L is the fiber length, and γ_0 is the Raman gain coefficient. Assuming $\gamma_0 = 5 \times 10^{-10}$ cm/W and a 200m long single mode fiber having a 6μm diameter, the critical power level is about 0.6W. As shown in Eqs. 1.1 and 1.2, the Raman scattering is independent of the signal frequency, but the quantum noise is linearly proportional to the signal bandwidth. Therefore, the optical dynamic range of optical fiber delay line decreases linearly with the increasing signal bandwidth. Fig 1.1 shows the

optical dynamic range according to signal bandwidth. As shown in the figure, the dynamic range of 10GHz signal along a 200m delay line exceeds 80dB.

The last advantage of optical delay line is its compact size. This is shown clearly in Table 1.1. It is possible to make signal processing components be compact due to small size of optical fiber delay line.

Because of these advantages, the optical delay line has wide applications. For example, in area of radio frequency (RF) photonics, the optical delay line is able to apply for phased array antennas. If RF phase shifters are used in the array antenna systems, beam squinting problem is unavoidable because RF phase shifters are dependent of input frequency. However, optical delay line is

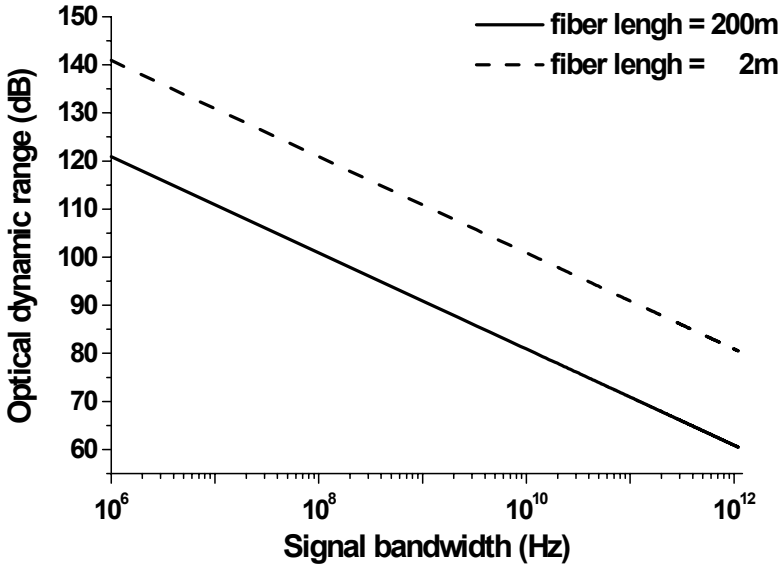

Figure 1.1 Optical dynamic range with modulation signal bandwidth.

independent of the modulation frequency, thus the beam squinting problem is negligible [4]. Another example is optical buffering, to delay data until it is ready to be processed [5].

In this thesis, the tunable fiber-optic microwave filter, which is important application of optical delay lines, is demonstrated.

In the Chapter Ⅱ, the background of optical delay lines is reviewed, and in Chapter Ⅲ, the previous methods to configure the microwave filters using optical delay line and their problems are discussed on. In Chapter IV, a new structure using four-mode dispersion compensation fiber (DCF) is proposed. In Chapter V, this thesis is concluded.

Table 1.1. Size comparison between fiber and coaxial cable.

	Fiber	Coaxial cable
Diameter	0.2 mm	5 mm
Weight	0.073 g/m	30~100 g/m

Ⅱ. Background

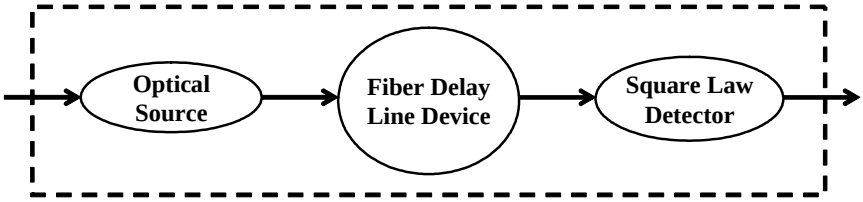

Figure 2.1 Generalized fiber-optic signal processing system

A generalized fiber optic signal processing system including an optical source, an optical fiber delay-line device, and a detector is shown Fig. 2.1. In this structure, the optical source is directly modulated and the modulated signal is detected by a photo diode after passing through the delay line device. The structure of this system depends on the type of the optical delay line device.

The optical fiber delay line device can be divided into two classes [2]: recirculating delay line and nonrecirculating, or tapped delay line. The recirculating delay line is shown Fig. 2.2. This configuration is composed of a fiber loop in which length determines the time delay. The fiber loop is closed on itself and for controlling the delayed signal power, an attenuator is inserted in the loop. Fig. 2.3 shows the nonrecirculating delay line having several taps composed of delay lines and weight components. The delay line controls the

phase of input signal and the weight component controls the power of input signal. In this structure, the signals at one end of the delay lines are delayed and weighted, and then added either by optical summation before detection or by electronic summation after detection.

These delay lines, recirculating delay line and tapped delay line, can perform a number of signal-processing functions. For example, the recirculating delay lines can be used for applications requiring short-term storage of discrete or analog signals. The tapped delay lines can do many time-domain functions, such as convolution and correlation. Moreover, both can perform as microwave frequency filters whose modulation transfer functions are determined by Fourier transform of their response to a modulation impulse.

In this thesis, new tapped delay line filters is proposed, thus the next section is focused on the previously reported methods to configure the tapped delay line filters.

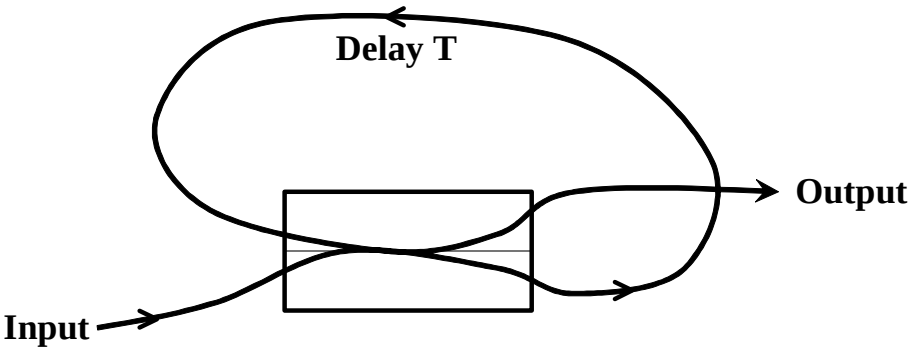

Figure 2.2 Recirculating delay line with loop delay T.

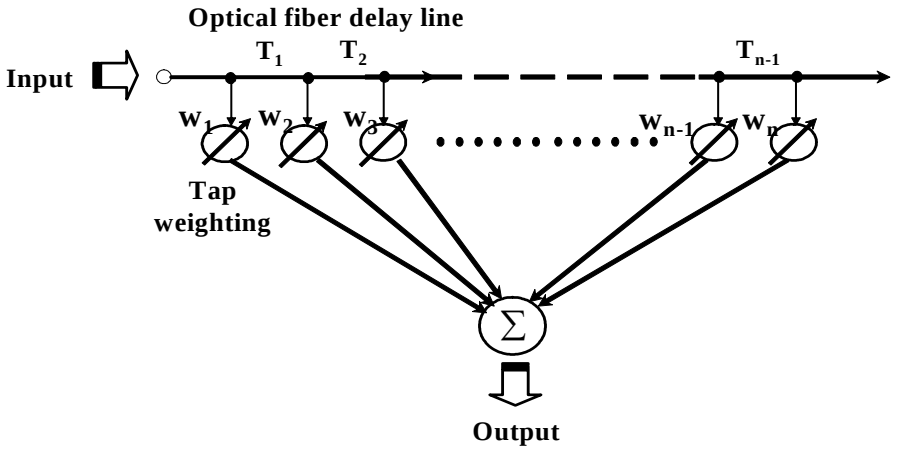

Figure 2.3 Tapped delay line with tap intervals T_m

and weighting elements W_m.

Ⅲ. Review of existing tapped delay line filters

The existing methods for realizing tunable microwave filters using optical delay lines can be classified into three techniques.

Firstly, it is to use several long high dispersive fibers (HDF). In this structure, the delay lines of taps are composed of several HDFs having different length and the weights of taps are controlled by attenuators [6]. Secondly, it is to make use of multiple sources and one HDF. The time delay in this filter is function of wavelength, the dispersion parameter, and the length of the HDF [7]. And lastly, it is to take advantage of multiple sources and one chirped fiber Bragg grating (CFBG). In this filter, the difference of the reflection locations within CFBG according to source wavelength determines the time delay and the output power of source controls the weight [8-9].

In this section, these three methods are reviewed in detail.

A. Fiber-optic filter using several fibers

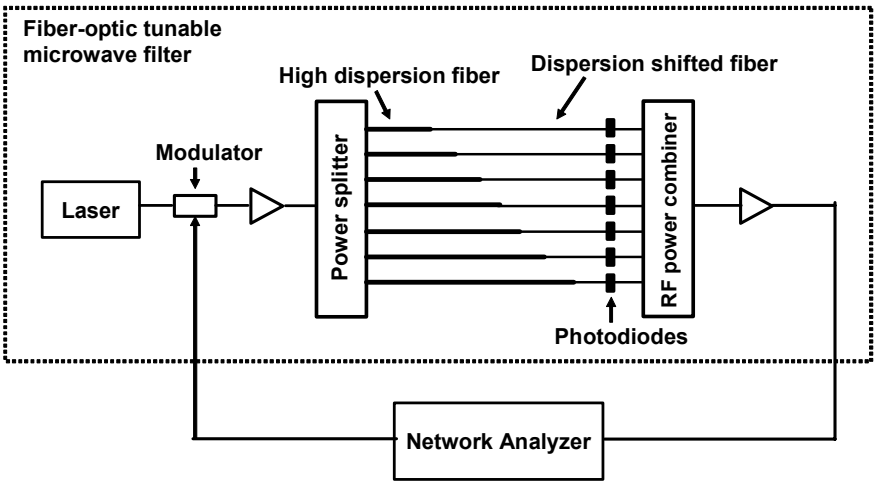

Figure 3.1 Fiber-optic filter using several HDFs.

The first method is to use several high dispersion fibers (HDF) and as many photo diodes as the number of HDFs. The filter configuration with seven taps is shown in Fig. 3.1. In this filter, the tap is composed of a source to be shared by all taps, a photo diode (PD), an optical attenuator and one fiber to be formed by a HDF and a dispersion-shifted fiber (DSF). The weight of this filter is controlled by an optical attenuator before the PD. In the configuration, the unit length of HDF is set at a fixed value and different combinations of the unit length are included into filter taps. The overall time delays of each tap are equalized at λ_0 by additional segments of DSF, thus the frequency response at this wavelength is flat. However, the time delay of each tap is tuned by the

source wavelength, because the dispersion of HDF and DSF is the function of the source wavelength.

The effective variable unit time delay, $\Delta\tau$, can be given as

$$\Delta\tau = \ell \cdot \int_0^{\Delta\lambda} (D_{HD}(\lambda) - D_{DS}(\lambda)) \cdot d\lambda \tag{3.1}$$

where $\Delta\lambda=\lambda-\lambda_0$, ℓ is the length of HDF, $D_{HD}(\lambda)$ and $D_{DS}(\lambda)$ are dispersion parameters of HDF and DSF. If the weight of all taps is equal, the amplitude response of this FIR filter is then obtained from the next relation

$$A(f) = \left| \sum_{n=1}^{N} e^{j2\pi k_n (f/f_s)} \right| \tag{3.2}$$

where k_n is the number of unit length of HDF in tap n, and $f_s=1/\Delta\tau$.

In this filter, the tuning of the filter response can be easily controlled by changing the source wavelength. However, for increasing tap numbers using this method, high dispersion fibers, photo diodes and attenuators are required as many as the increased tap number. This fact can be a seriously problem in expanding the filter taps for obtaining desired filter response.

B. Fiber-optic filter using multiple sources

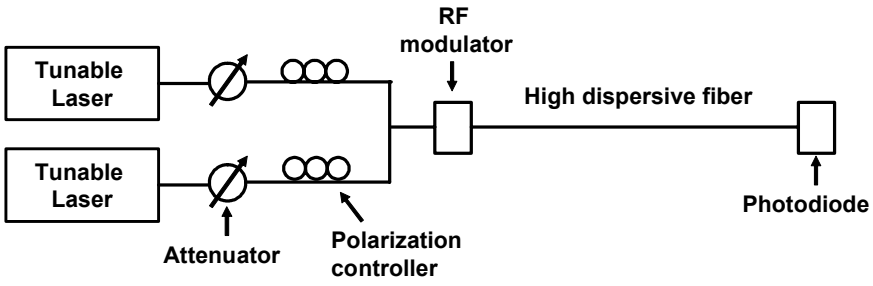

Figure 3.2 Fiber-optic filters with two optical sources.

The second method is to use multiple sources and one high dispersion fiber. Fig. 3.2 shows the experimental setup of two tap delay line filter to be composed of a tunable laser diode, a RF modulator, a single length of high dispersion fiber and a detector. In this filter, the each tap consists of one tunable source, one attenuator, and one HDF to be shared by all taps. The optical attenuator behind the tunable laser controls the signal power, the weight of the tap, and the time delay can be produced by the wavelength difference of the two tunable sources and dispersion of HDF. The amount of time delay can be expressed as

$$\Delta t = \Delta \lambda DL \tag{3.3}$$

where $\Delta\lambda$ is wavelength difference, D is the dispersion parameter of HDF and L is HDF length. The time delay can be changed by tuning the value of $\Delta\lambda$.

This filter uses separated lightwave sources, so the coherence problem is not happened. However, the tap number is same with the source number, thus more sources are needed for increasing the tap number.

C. Fiber-optic filter using chirped gratings

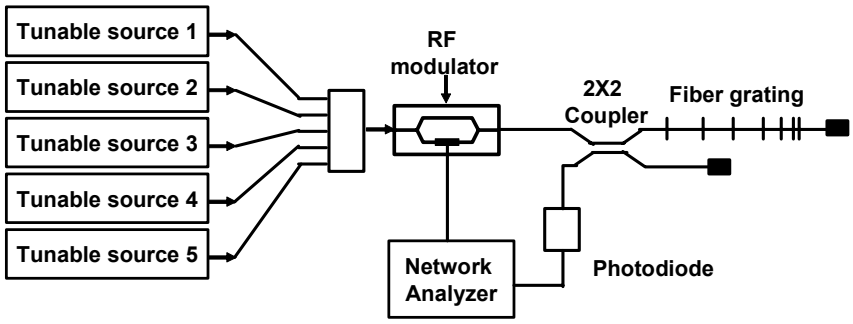

Figure 3.3 Fiber-optic filter using chirped fiber grating.

The third method is to take advantage of multiple sources and one chirped fiber grating. Fig 3.3 shows the 5 tap filter using this method. In this filter, one source and one grating to be shared by all taps make one tap. The difference of the reflection point within the grating according to source wavelength determines the time delay and the source output power controls the weight.

To get the time delay using fiber gratings is a very simple technique, and it is possible to make the filter more compact. However, this technique has a weak point that the as many sources are required as taps.

We have review three methods to configure the tunable fiber-optic microwave filters. As mentioned early, for increasing tap numbers using these three techniques, sources or high dispersion fibers must be required as many as the increased tap number. In the next chapter, a new tunable filter that can overcome this disadvantage is proposed.

Ⅳ. A new proposed tunable microwave filter using four modes dispersion compensation fiber

In this chapter, to overcome the disadvantage of existing methods, we propose a novel fiber-optic filter composed of two mode converters, which are made of a dispersion compensation fiber (DCF) guiding four fiber modes and a hollow optical fiber (HOF), and one tunable source having broad linewidth. Fig. 4.1 shows the configuration of this filter. This proposed filter uses the velocity difference among fiber modes to make delay lines of taps and uses the coupling ratio among modes to control the weight of taps. The number of modes guided within the DCF means tap numbers, thus the tap number can be easily increased by replacing the DCF with other DCF guiding more fiber modes without additions of sources or fibers. Moreover, the time delay between modes can be easily controlled by tuning the incident light wavelength because the velocity of fiber modes is dependent on the source wavelength. For detailed explanation of this filter, this chapter is divided into three sections. In section A, the characteristic of DCF modes will be analyzed and discussed the simulation results, in section B, the measured time delay produced by velocity difference between modes will be shown, and section C will focus on the simulated and measured filter characteristic.

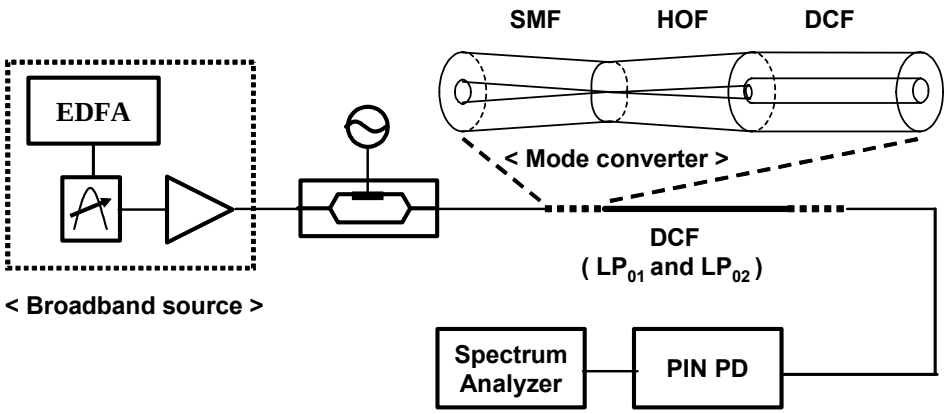

Figure 4.1 Configuration of new proposed fiber-optic microwave tunable filter.

A. The analysis of fiber modes within dispersion compensation fiber (DCF) and simulation results

As mentioned early, the proposed filter uses fiber modes within DCF to realize delay lines. Therefore, it is very important to have knowledge of the characteristics of fiber modes. For analyzing the fiber modes, this section is divided into four parts:

A.1) Find guided modes within DCF from Maxwell's equations

A.2) Numerical solution for mode index of the guided mode

A.3) The calculation of time delay to be within DCF

A.4) The hollow optical fiber to control the coupling ratio between modes

A.1) Find guided modes within DCF from Maxwell equations

This part focuses on the analysis of the fiber modes guided in the DCF having step index profile. Before the analysis of fiber, which is a circular waveguide with a step index fiber, it is assumed that the radius of the fiber's cladding is sufficiently large so that the field inside this cladding decreases exponentially and becomes zero at the air-cladding interface.

First of all, it should be found that the wave equations in cylindrical

coordinates from Maxwell's equations. Assuming a linear isotropic dielectric material without currents and free charges, Maxwell's equations take the form [10]

$$\nabla \times E = -\frac{\partial B}{\partial t} \tag{4.1a}$$

$$\nabla \times H = \frac{\partial D}{\partial t} \tag{4.1b}$$

$$\nabla \cdot D = 0 \tag{4.1c}$$

$$\nabla \cdot B = 0 \tag{4.1d}$$

where D=εE and B=μH. The parameter ε is the permittivity and μ is permeability of the medium. If electromagnetic waves propagate along the z axis, they can be expressed the following way:

$$E = E_0(r,\phi)e^{j(wt-\beta z)} \tag{4.2a}$$

$$H = H_0(r,\phi)e^{j(wt-\beta z)} \tag{4.2b}$$

which are harmonic in time t and coordinate z. The parameter β is the z component of the propagation vector. The value will be determined by the boundary conditions at the interface between core and cladding.

When Eqs. 4.2a and 4.2b are substituted into Maxwell's curl equations 4.1a, we have the following equations:

$$\frac{1}{r}(\frac{\partial E_z}{\partial \phi} + jr\beta E_\phi) = -jw\mu H_r \tag{4.3a}$$

$$j\beta E_r + \frac{\partial E_z}{\partial r} = jw\mu H_\phi \tag{4.3b}$$

$$\frac{1}{r}[\frac{\partial}{\partial r}(rE_\phi) - \frac{\partial E_r}{\partial \phi}] = -jw\mu H_z \tag{4.3c}$$

and, from Maxwell's curl equations 4.1b,

$$\frac{1}{r}(\frac{\partial H_z}{\partial \phi} + jr\beta H_\phi) = jw\varepsilon E_r \tag{4.3d}$$

$$j\beta H_r + \frac{\partial H_z}{\partial r} = -j\varepsilon w E_\phi \tag{4.3e}$$

$$\frac{1}{r}[\frac{\partial}{\partial r}(rH_\phi) - \frac{\partial E_r}{\partial \phi}] = j\varepsilon w E_z \tag{4.3f}$$

From these six equations, the transverse field components (E_r, E_φ, H_r, and H_φ) are obtained as follows:

$$E_r = -\frac{j}{q^2}(\beta\frac{\partial E_z}{\partial r} + \frac{\mu\omega}{r}\frac{\partial H_z}{\partial \phi}) \tag{4.4a}$$

$$E_\phi = -\frac{j}{q^2}(\frac{\beta}{r}\frac{\partial E_z}{\partial \phi} - \mu\omega\frac{\partial H_z}{\partial r}) \tag{4.4b}$$

$$H_r = -\frac{j}{q^2}(\beta\frac{\partial H_z}{\partial r} - \frac{\varepsilon\omega}{r}\frac{\partial E_z}{\partial \phi}) \tag{4.4c}$$

$$H_\phi = -\frac{j}{q^2}(\frac{\beta}{r}\frac{\partial H_z}{\partial \phi} + \omega\varepsilon\frac{\partial E_z}{\partial r}) \tag{4.4d}$$

where $q^2 = w^2\varepsilon\mu - \beta^2 = k^2 - \beta^2$.

Substitution of Eqs. 4.4c and 4.4d into Eq. 4.3f results in the wave equation in cylindrical coordinates,

$$\frac{\partial^2 E_z}{\partial r^2} + \frac{1}{r}\frac{\partial E_z}{\partial r} + \frac{1}{r^2}\frac{\partial^2 E_z}{\partial \phi^2} + q^2 E_z = 0 \tag{4.5a}$$

and substitution of Eqs. 4.4a and 4.4b into Eq. 4.3c results in

$$\frac{\partial^2 H_z}{\partial r^2} + \frac{1}{r}\frac{\partial H_z}{\partial r} + \frac{1}{r^2}\frac{\partial^2 H_z}{\partial \phi^2} + q^2 H_z = 0 \tag{4.5b}$$

In order to solve these equations, in this thesis, the separation-of-variables method is used. A solution of the form is assumed as

$$E_z = AF_1(r)F_2(\phi)F_3(z)F_4(t) \tag{4.6}$$

However, from Eqs. 4.2a and 4.2b, the time and z-dependent factors are given by

$$F_3(z)F_4(t) = e^{j(wt-\beta z)} \tag{4.7}$$

Moreover, the field component can not be changed when the coordinate φ is increased by 2л because of the circular symmetry of the waveguide. Therefore, it can be assigned a periodic function of the form

$$F_2(\phi) = e^{jv\phi} \tag{4.8}$$

The constant v can be positive or negative, but it must be an integer since the fields must be periodic in φ with a period of 2л.

From Eqs. 4.5a, 4.6, 4.7, and 4.8, the wave equation for E_z becomes

$$\frac{\partial^2 F_1}{\partial r^2} + \frac{1}{r}\frac{\partial F_1}{\partial r} + (q^2 - \frac{v^2}{r^2})F_1 = 0 \qquad (4.9)$$

which is differential equation for Bessel functions. With the same approach, an equation for H_z can be derived.

Eq. 4.9 can be solved for two regions inside and outside the core. In the core, the field must be remain finite as r → 0, therefore it can be expressed the filed form as

$$E_z(r < a) = AJ_v(ur)e^{jv\phi}e^{j(wt-\beta z)} \qquad (4.10a)$$

$$H_z(r < a) = BJ_v(ur)e^{jv\phi}e^{j(wt-\beta z)} \qquad (4.10b)$$

where $u^2 = k_1^2 - \beta^2$ with $k_1 = 2\pi n_1 / \lambda$, a is core radius, and A, B are arbitrary constants.

Outside of the core, the field must decrease to zero as r → ∞, thus the field can be written like this

$$E_z(r > a) = CK_v(wr)e^{jv\phi}e^{j(wt-\beta z)} \qquad (4.10c)$$

$$H_z(r>a) = DK_v(wr)e^{jv\phi}e^{j(wt-\beta z)} \tag{4.10d}$$

where $w^2 = \beta^2 - k_2^{\,2}$ with $k_2 = 2\pi n_2 / \lambda$, and C, D are arbitrary constants.

Until now, we have found the field expressions of guided modes in step index fiber. Finally, to determine the propagation constant, β, of each mode, the boundary conditions at the core-cladding interface should be applied. The boundary conditions require that the tangential components of E field (E_φ and E_z) must be continued inside and outside of the dielectric interface at the r=a.

For z component of E-field, from Eqs. 4.10a and 4.10c, the next condition can be derived

$$(E_z)_{core} = (E_z)_{cladding} \qquad r = a \tag{4.11a}$$

$$(E_z)_{core} - (E_z)_{cladding} = AJ_v(ua) - Ck_v(wa) = 0 \tag{4.11b}$$

Likewise, for the z component of H-filed, next condition can be wrote like as,

$$(H_z)_{core} = (H_z)_{cladding} \qquad r = a \tag{4.12a}$$

$$(H_z)_{core} - (H_z)_{cladding} = BJ_v(ua) - Dk_v(wa) = 0 \tag{4.12b}$$

Then, from Eqs. 4.10a, 4.10b, and 4.4b, the condition of E-field φ

component is given by

$$(E_\phi)_{core} = (E_\phi)_{cladding} \qquad r = a \tag{4.13a}$$

$$(E_\phi)_{core} - (E_\phi)_{cladding} = -\frac{j}{u^2}[A\frac{jv\beta}{a}J_v(ua) - B\omega\mu uJ_v'(ua)] - \frac{j}{w^2}[C\frac{jv\beta}{a}K_v(wa) - D\omega\mu wK_v'(wa)] = 0 \tag{4.13b}$$

Similarly, the condition of H-field φ component is shown that

$$(H_\phi)_{core} = (H_\phi)_{cladding} \qquad r = a \tag{4.14a}$$

$$(H_\phi)_{core} - (H_\phi)_{cladding} = -\frac{j}{u^2}[B\frac{jv\beta}{a}J_v(ua) + A\omega\varepsilon_1 uJ_v'(ua)] - \frac{j}{w^2}[D\frac{jv\beta}{a}K_v(wa) + C\omega\varepsilon_2 wK_v'(wa)] = 0 \tag{4.14b}$$

These four equations to be determined by boundary conditions are as follows.

$$AJ_v(ua) + B\cdot 0 - Ck_v(wa) + D\cdot 0 = 0 \tag{4.15a}$$

$$A(\frac{j}{u^2}\frac{jv\beta}{a}J_v(ua)) + B(\frac{j}{u^2}\omega\mu uJ_v'(ua)) + C(\frac{j}{w^2}\frac{jv\beta}{a}K_v(wa)) + D(\frac{j}{w^2}\omega\mu wK_v'(wa)) = 0 \tag{4.15b}$$

$$A\cdot 0 + BJ_v(ua) + C\cdot 0 - Dk_v(wa) = 0 \tag{4.15c}$$

$$A(-\frac{j}{u^2}\omega\varepsilon_1 uJ_v'(ua)) + B(\frac{j}{u^2}\frac{jv\beta}{a}J_v(ua)) \\ -C(\frac{j}{w^2}\omega\varepsilon_2 wK_v'(wa)) + D(\frac{j}{w^2}\frac{jv\beta}{a}K_v(wa)) = 0 \tag{4.15d}$$

As shown in the equations (4.15a-4.15d), theses equations are with four unknown coefficients, A, B, C, D. The solution exists only if the determinant of these coefficients is null:

$$\begin{vmatrix} J_v(ua) & 0 & -K_v(wa) & 0 \\ \frac{\beta v}{au^2}J_v(ua) & \frac{j\omega\mu}{u}J_v'(ua) & \frac{\beta v}{aw^2}K_v(wa) & \frac{j\omega\mu}{w}K_v'(wa) \\ 0 & J_v(ua) & 0 & -K_v(wa) \\ -\frac{j\omega\varepsilon_1}{u}J_v'(ua) & \frac{\beta v}{au^2}J_v(ua) & -\frac{j\omega\varepsilon_2}{w}K_v'(ua) & \frac{\beta v}{aw^2}K_v(wa) \end{vmatrix} = 0$$

The result of this 4×4 determinant calculation is the following characteristic equation:

$$(\frac{J_v'(ua)}{uJ_v(ua)} + \frac{K_v'(wa)}{wK_v(wa)})(k_1^2\frac{J_v'(ua)}{uJ_v(ua)} + k_2^2\frac{K_v'(wa)}{wK_v(wa)}) \\ = (\frac{\beta v}{a})^2(\frac{1}{u^2}+\frac{1}{w^2})^2 \tag{4.16}$$

The propagation constant of each guided mode can be determined from this characteristic equation, when source wavelength, core radius, and refractive index values of core and cladding are given. However, the exact analysis of the

characteristic equation is mathematically very complex. Thus, if the difference of refractive index between core and cladding is very small, for simpler calculations, weakly guiding fiber approximation can be applied. In this approximation, the filed pattern and propagation constants of some modes are very similar. For example, these modes, $\{TE_{02}, TM_{02}, HE_{22}\}$, have similar propagation constant, thus these modes can be combined by new degenerated mode. Gloge call such degenerated modes linearly polarized (LP) modes [11]. In general, the relationship between linearly polarized modes and TE, TM, EH, HE modes is following

1. Each LP_{0m} mode is from each HE_{1m} mode.
2. Each LP_{1m} mode is induced from TE_{0m}, TM_{0m} and HE_{2m} modes.
3. Each LP_{vm} mode ($v \geq 2$) comes from $HE_{v+1,m}$ and $EH_{v-1,m}$ mode.

In the weakly guiding condition, the characteristic equation is changed into the next form

$$\frac{uJ_{j-1}(ua)}{J_j(ua)} = -\frac{wK_{j-1}(wa)}{K_j(wa)} \tag{4.17}$$

where

$$j = \begin{cases} 1 & \textit{for TE and TM} \text{ modes} \\ v+1 & \textit{for EH} \text{ modes} \\ v-1 & \textit{for} \text{ HE modes} \end{cases}$$

A.2) Numerical solution for the guided modes

In this section, the numerical solution for the characteristic equation (Eq. 4.17) will be found. At the numerical calculation, it is assumed that the dispersion compensation fiber (DCF) refractive index difference between core and cladding is about 2.88% and the radius of core is 3.54μm. The number of guided modes can be calculated from cutoff frequency of modes and the normalized frequency (V)

$$V = \frac{2\pi}{\lambda} a \sqrt{n_1^2 - n_2^2} \tag{4.18}$$

where a is the radius of core, λ is the wavelength of the guided field and n_1 , n_2 are refractive indices of core and cladding. In this structure, the DCF has four modes (LP_{01}, LP_{11}, LP_{21}, and LP02) in the wavelength range from 1530nm to 1570nm. However, in the proposed fiber-optic filter scheme shown in Fig. 4.1, only LP_{01} and LP_{02} modes are excited within the DCF, because mode orthogonality between LP_{01} mode and LP_{11}, LP_{21} modes. Details are given in the next section.

The effective index values of LP_{01} and LP_{02} to be obtained from Eq. 4.17 are shown in Fig. 4.2 (a) and (b). These vales are the simulation results. As shown these figures, although the effective index of LP_{01} is lager than that of LP_{02}, the LP_{02} index slope according to wavelength is lager than LP_{01}.

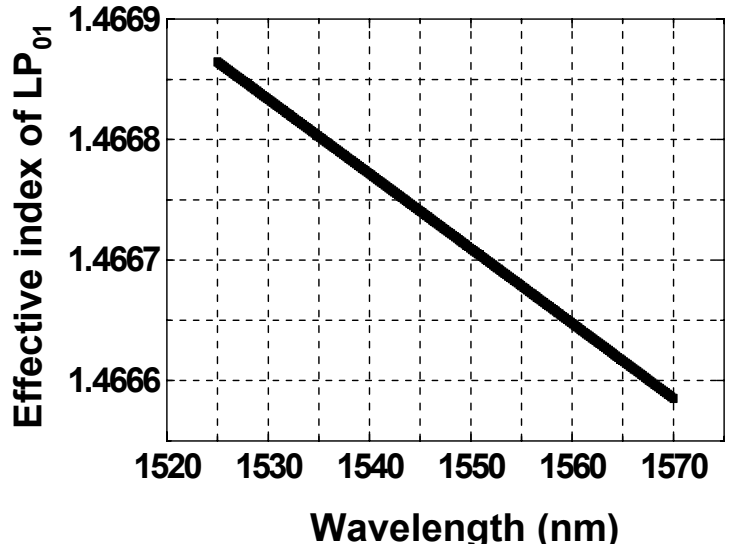

(a)

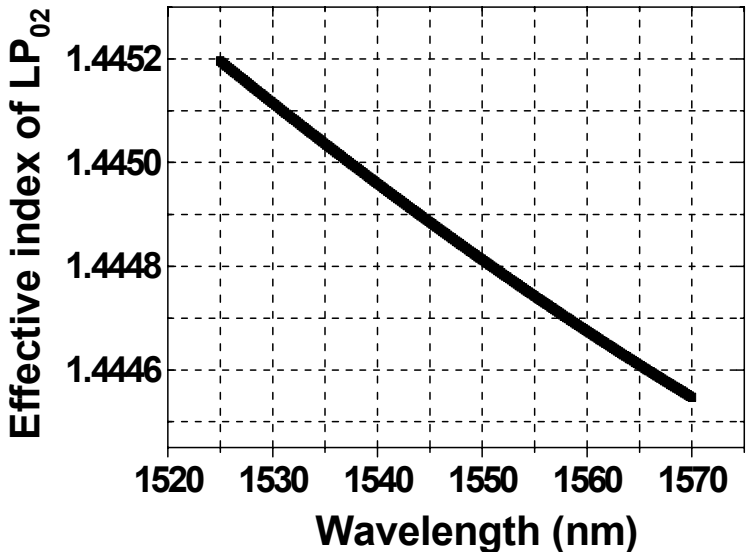

(b)

Figure 4.2 Effective indices of (a) LP_{01} mode and (b) LP_{02} mode within dispersion compensation fiber (DCF).

A.3) Calculation of time delay to be produced within DCF

The velocity of LP_{01} mode is different from that of LP_{02} within the DCF, therefore the time delay is happened at the end of the DCF.

The group velocity of guided mode can be computed as

$$v_g = \left(\frac{d\beta}{d\omega}\right)^{-1}$$
$$= \left(\frac{d}{d\omega}(n_{eff} \cdot k_0)\right)^{-1} = \left(\frac{k_0 dn_{eff}}{d\omega} + \frac{n_{eff} dk_0}{d\omega}\right)^{-1} = \left(-\frac{\lambda}{c}\frac{dn_{eff}}{d\lambda} + \frac{n_{eff}}{c}\right)^{-1} \quad (4.19)$$

where $k_0 = 2\pi / \lambda$.

From Eq. 4.19 the group velocity of LP_{01} and LP_{02} modes can be obtained and Fig. 4.3 (a) and (b) show the reciprocal value of the group velocity.

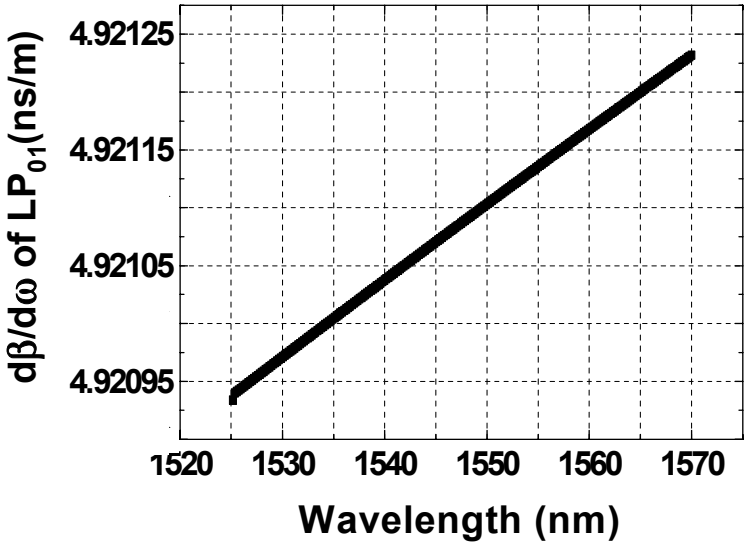

(a)

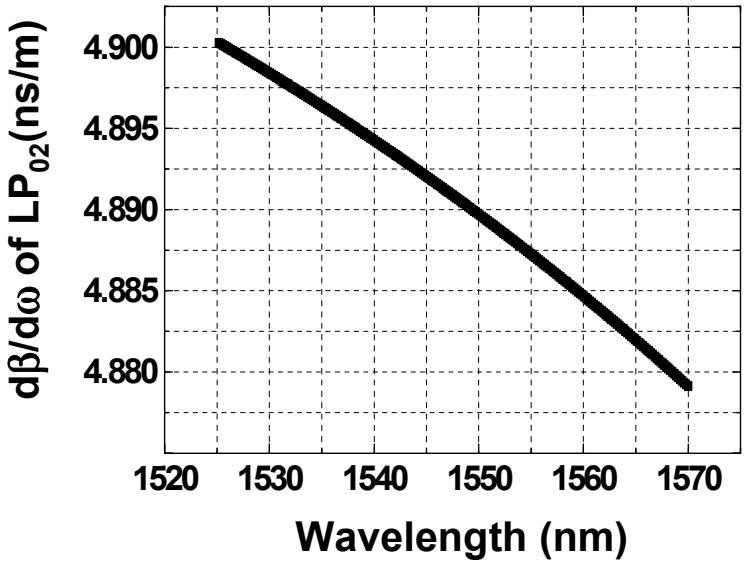

(b)

Figure 4.3 $d\beta / d\omega$ **of (a) LP_{01} mode and (b) LP_{02} mode within DCF.**

The time delay to be induced by velocity difference between LP_{01} and LP_{02} modes can be expressed like that

$$\Delta T = ((\frac{d\beta}{dw})_{LP02} - (\frac{d\beta}{dw})_{LP01})L = ((n_g)_{LP02} - (n_g)_{LP01})\frac{L}{c}$$

where β is propagation constant, n_g is group index within DCF and L is DCF length. This time delay is dependent on the source wavelength and the waveguide structure of DCF such as core radius (d) and the relatively index difference between core and cladding ($\Delta = (n_1 - n_2)/n_2$, where n_1 is core index and n_2 is cladding index). The calculated results are shown in Fig. 4.4 and Fig. 4.5. Fig. 4.4 shows the time delay as a function of Δ and d at fixed wavelength of 1530nm. Fig. 4.5(a) shows the time delay as a function of the source wavelength and Δ at fixed value of d=3.5μm and Fig. 4.5(b) shows the time delay as a function of the source wavelength and d at fixed value of Δ=2.0%. It is clearly shown that the time delay is continuously tunable. From these results, proper values of core radius and relatively index difference can be determined to obtain desired amount of the time delay.

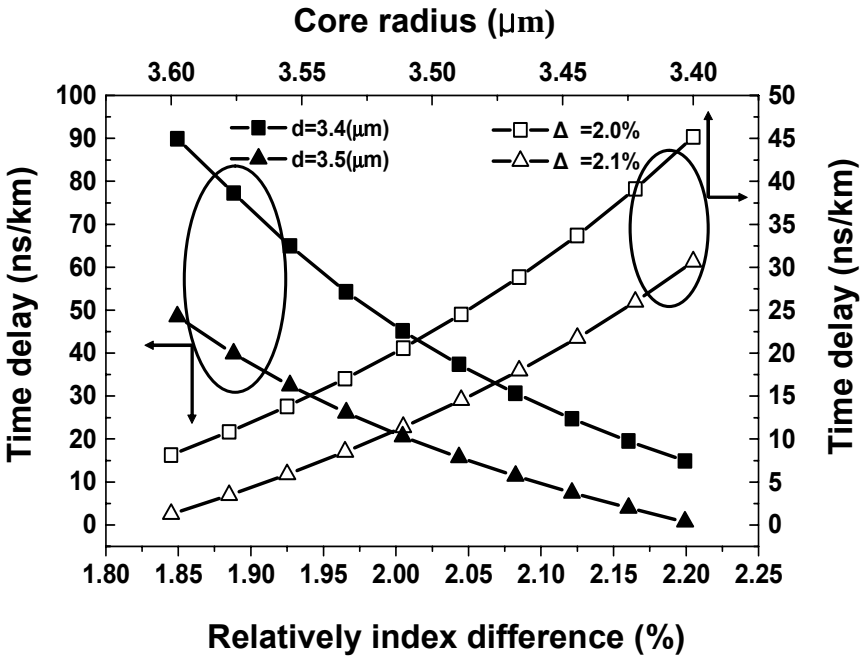

Figure 4.4 Time delay between LP01 and LP02 modes within DCF.

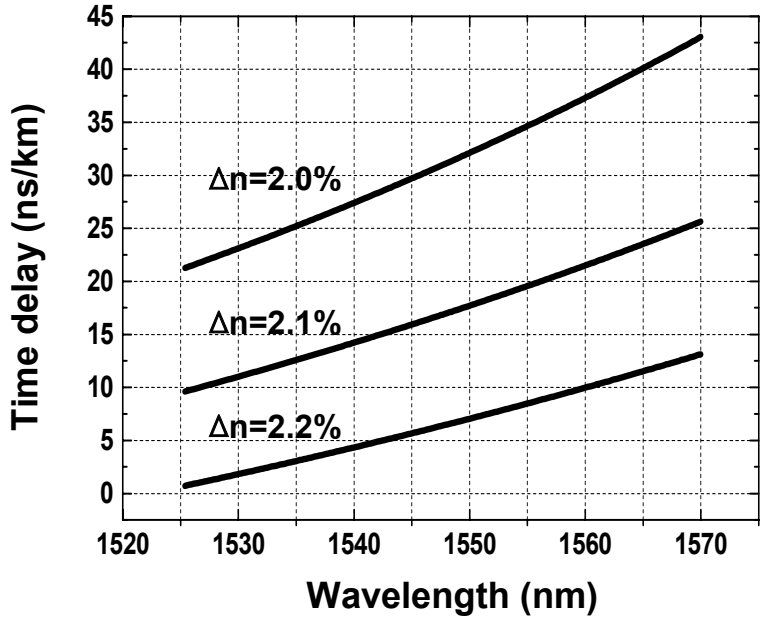

Figure 4.5 (a) Calculated results of the time delay within DCF as a function of the source wavelength and relatively index difference at fixed core radius (3.5μm).

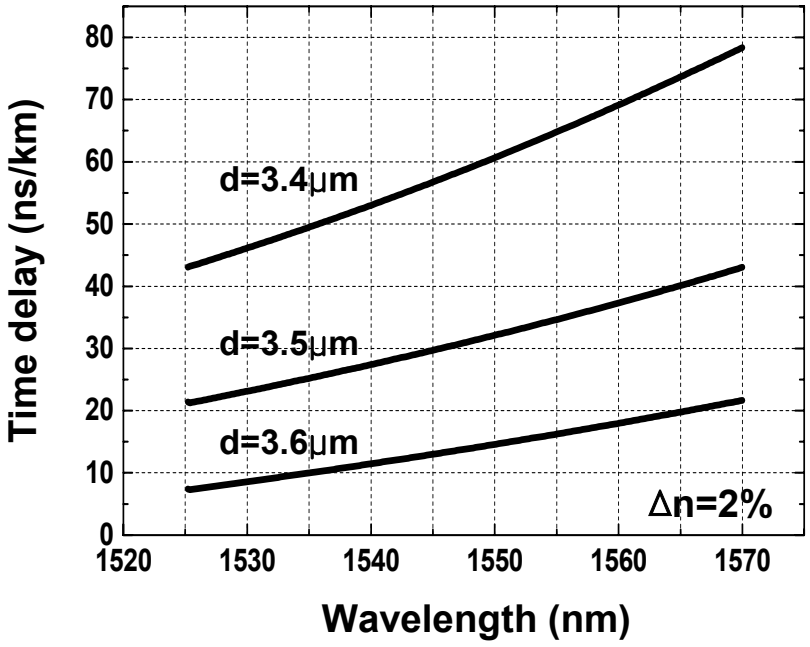

Figure 4.5(b) Calculated results of the time delay within DCF as a function of the source wavelength and core radius at fixed relative index difference (2.0%).

A.4) The hollow optical fiber (HOF) to control the coupling ratio between modes

Until now, we have focused on the time delay in DCF. In this section, we explain the way to control the weight of each tap, which is one of key issues with delay lines in configuration tapped delay line filters.

In this proposed filter, to control the weight of each tap, we should control the power of excited modes in DCF. It is difficult to change the mode power individually, after separating each mode from several modes to be excited in one fiber, therefore the mode power can be controlled by changing the coupling ratio into the DCF modes. For this work, we use the hollow optical fiber (HOF). As shown in Fig.4.1, the HOF is inserted between single mode fiber (SMF) and DCF for controlling the coupling ratio among excited modes in DCF.

The fundamental mode (LP_{01}) of SMF is changed into the ring-shape fundamental mode at the end of the HOF, and the power of the ring shape LP_{01} mode is transferred guided modes within the DCF. The power coupling efficiency (κ) into each mode can be computed by overlap integral between E-field mode of HOF and H-field mode to be guided in DCF. The efficiency can be expressed as [12]

$$\kappa = \left| \iint E_{LP01(HOF)} \times H^{*}_{\text{excited mode (DCF)}} r dr d\theta \right|^2 / \left(\left| \iint E_{LP01(HOF)} \times H_{LP01(HOF)} r dr d\theta \right| \cdot \left| \iint E^{*}_{\text{excited mode (DCF)}} \times H^{*}_{\text{excited mode (DCF)}} r dr d\theta \right| \right) \quad (4.20)$$

The coupled power into LP_{11}, LP_{21} modes of DCF from LP_{01} mode of HOF is zero by Eq.4.20. It means that LP_{11}, LP_{21} modes and LP_{01} mode are orthogonal. Thus, only LP_{01} and LP_{02} modes are excited in DCF. The power transferred to each of two modes (LP_{01} and LP02) depends on the hole radius of HOF and the wavelength of the mode [12]. The power coupling efficiency according to hole radius of HOF is shown at Fig. 4.6. This simulation result is assumed that the wavelength is 1550nm, the radius of DCF core is 3.6μm and refractive index difference between core and cladding is 2.02%.

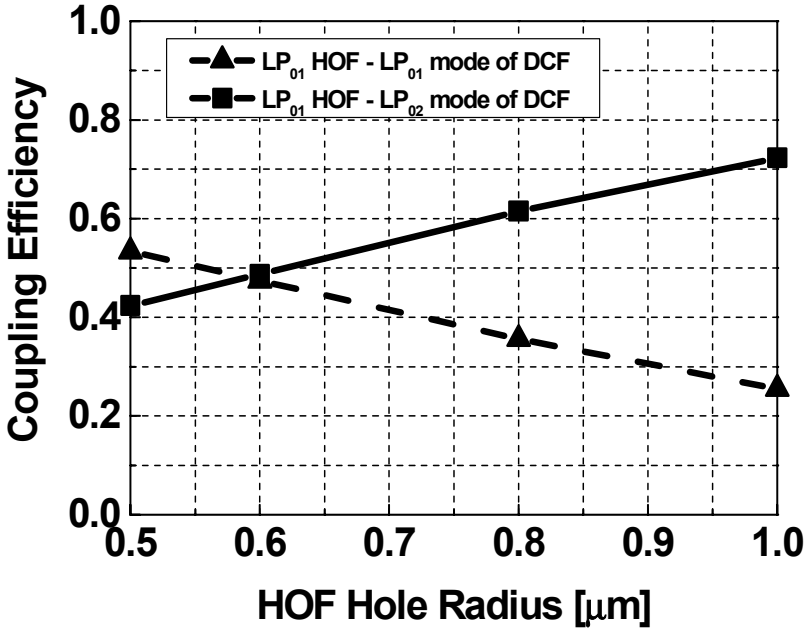

Figure 4.6 Coupling efficiency of LP_{01}, LP_{02} modes.

B. The experimental result of time delay induced by velocity difference between modes

In the section A, we calculated the time delay to be induced within DCF from wave equations. Now we measured the time delay using the experimental setup shown in Fig. 4.7. The source is distributed feedback laser (DFB) which is operated at the wavelength 1530nm. The source is gain switched by 500MHz RF signal at the threshold bias, thus the output signal becomes optical pulse having 2ns repetition rate. The pulse is detected by the PIN PD after passing through the DCF and the detected RF pulse is displayed at the sampling oscilloscope. In Fig. 4.8 (a) and (b), the detected pulses without DCF and with DCF are shown, respectively. The second peak appeared in the one pulse is generated due to relaxation oscillation of the semiconductor laser diode. As shown Fig. 4.8 (b), the delayed RF pulse is measured, and the delay is about 1ns. In the figure, the power of the delayed pulse is not same as the power of the original pulse, because the power ratio to be transferred the each mode is not same. It can be improved by changing the hole radius of HOF.

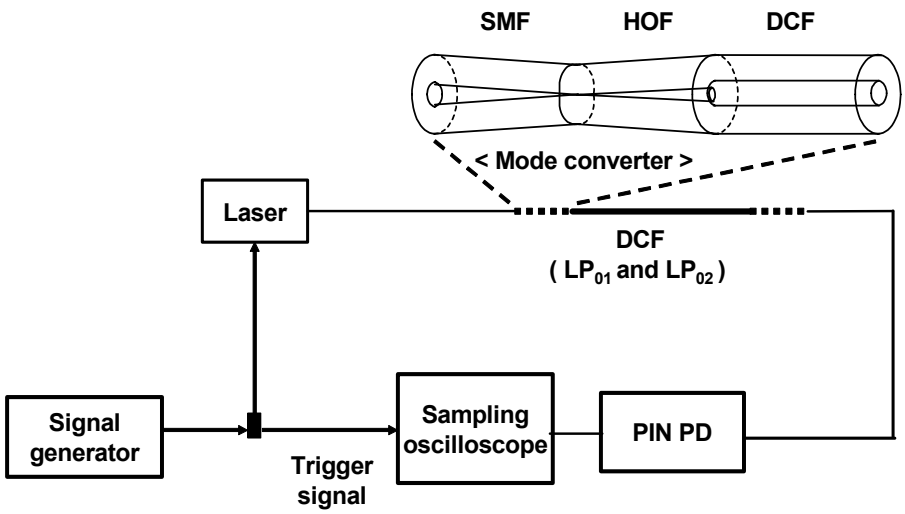

Figure 4.7 Experimental setup for measuring the time delay induced within DCF.

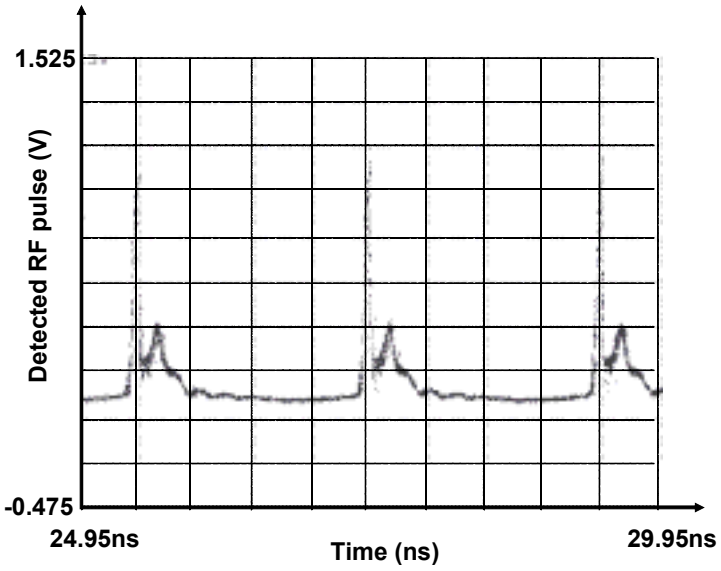

(a)

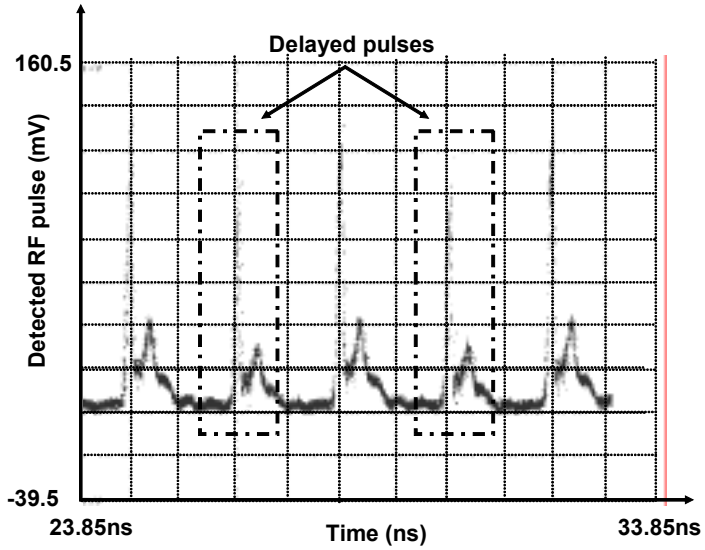

(b)

Figure 4.8 Time delay with (a) and without (b) DCF.

C. The proposed filter characteristics

We measure the frequency response of the proposed filter from the experimental setup shown in Fig. 4.1. As shown the figure, the source output is intensity modulated by electro-optic modulator and the modulated signal is fed into the mode converter which consists of single mode fiber (SMF), hollow optical fiber (HOF) and dispersion compensation fiber (DCF). At the front of DCF, two modes are excited and these modes propagate through the DCF. At the end of DCF, the time delay occurs because of the velocity difference between these modes. And lastly, these two modes are converted to fundamental mode (LP_{01}) of SMF by second mode converter and enter into the photo diode. In fact, this second mode converter is not needed, if the photo diode is not pigtailed with single mode fiber (SMF).

The input filed (E_{in}) of DCF can be expressed as

$$E_{in}(t)=\begin{bmatrix} \alpha E_{LP_{01}}(t) \\ (1-\alpha)E_{LP_{02}}(t) \end{bmatrix}=\begin{bmatrix} \alpha(e^{jw_o t}+\frac{1}{2}e^{j(w_o+w_c)t}+\frac{1}{2}e^{j(w_o-w_c)t}) \\ (1-\alpha)(e^{jw_o t}+\frac{1}{2}e^{j(w_o+w_c)t}+\frac{1}{2}e^{j(w_o-w_c)t}) \end{bmatrix} \tag{4.21}$$

where α is the ratio of power transferred to the LP_{01} mode, ω_0 is optical carrier frequency, ω_c is modulation frequency. The transformation matrix (T) of DCF can be expressed as

$$T = \begin{bmatrix} e^{-j\beta_{01}l} & 0 \\ 0 & e^{-j\beta_{02}l} \end{bmatrix} \tag{4.22}$$

where β_{0i} is the propagation constant of LP_{0i} mode, and ℓ is DCF length. The output filed (E_{out}) of the DCF are then given by

$$\begin{aligned} E_{out}(t) &= T \cdot E_{in}(t) \\ &= \begin{bmatrix} \alpha(e^{j(w_o t-\beta_{01}l)} + \frac{1}{2}e^{j((w_o+w_c)t-\beta_{01}l-\beta'_{01}lw_c)} + \frac{1}{2}e^{j((w_o-w_c)t-\beta_{01}l+\beta'_{01}lw_c)}) \\ (1-\alpha)(e^{j(w_o t-\beta_{02}l)} + \frac{1}{2}e^{j((w_o+w_c)t-\beta_{02}l-\beta'_{02}lw_c)} + \frac{1}{2}e^{j((w_o-w_c)t-\beta_{01}l+\beta'_{01}lw_c)}) \end{bmatrix} \end{aligned} \tag{4.23}$$

In the Eq. 4.23, the propagation constant is expended in a Taylor series around the carrier frequency up to second term as

$$\beta_{0i}(w) \approx \beta_{0i} + \beta'_{0i}(w-w_o) + \frac{1}{2}\beta''_{oi}(w-w_o)^2 + \ldots$$

The optical power to be detected by photo diode

$$P_{opt} = R \cdot E_{out} \times E^*_{out} \tag{4.24}$$

If α is 0.5, the optical power is expressed by

$$P_{opt} \propto 8\cos(\frac{\beta'_{01}l - \beta'_{02}l}{2} \cdot w_c) \cdot \cos^2(\frac{\beta_{01}l - \beta_{02}l}{2} \cdot w_c) \tag{4.25}$$

This equation shows that the optical power depends on the difference between

first order derivatives of propagation constants and the difference between effective indices of the two modes. However, the effective index difference between two modes according to wavelength is within the range of about 10^{-4}, thus the effect to be related with optical power can be ignored. The Fig. 4.9 shows the effective index differences between the two modes.

Fig. 4.10 shows the simulation result of electrical power, which is square of the optical power, as a function of the modulation frequency. In this simulation, it is assumed that the DCF core radius is 3.54μm and relatively index difference is 1.97%. The electrical power is maximum when two modes are in-phase and is minimum when they are out of phase. This figure also shows that the free spectral range (FSR), reciprocal value of the time delay, can be controlled by changing the source wavelength. In the figure, the DCF length is about 46m, thus the time delay between LP_{01} and LP_{02} modes to be happened in the DCF is about 1ns at the source wavelength is 1530nm, and the FSR is about 1GHz. This FSR can be controlled by tuning the source wavelength. The tuning rate is about 0.388ns/km·nm, which can be calculated from the figure. Of course, the time delay and the slope depend on the waveguide structure of DCF. If the DCF is designed to have smaller refractive index difference between core and cladding or the diameter of the core is shorter, the time delay inside DCF will be longer, and the FSR will be shorter.

Fig. 4.11 shows the experimental result of the filter response. The

measured FSR is 1.0659GHZ at 1530nm of source wavelength, thus the induced time delay within DCF having length of 46m is about 0.93817ns (20.395ns/km). Moreover, the tuning of FSR is shown clearly in the figure. For example, the FSR is about 0.9537 GHz (22.79ns/km) at 1535nm, and 0.9350GHz (23.25ns./km) at 1540nm, thus the measured tuning rate is about 0.288ns/km·nm. In addition, the notch rejection is more than 20dB for wavelengths covered in the experiment. Comparing these results with the simulation results, it can be estimated that the DCF core radius is 3.58μm and the relatively index difference is 1.93%. This value is different from the design parameters (3.54μm, 1.97%) considered at simulation, thus the measured tuning rate is different from the calculated tuning rate (0.388 ns/km·nm).

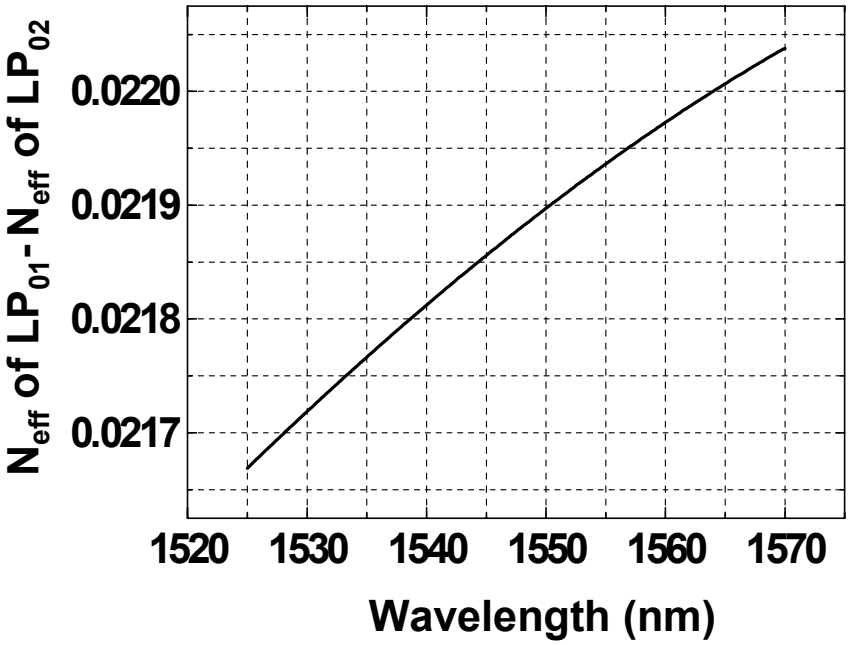

Figure 4.9 Effective index differences between two modes.

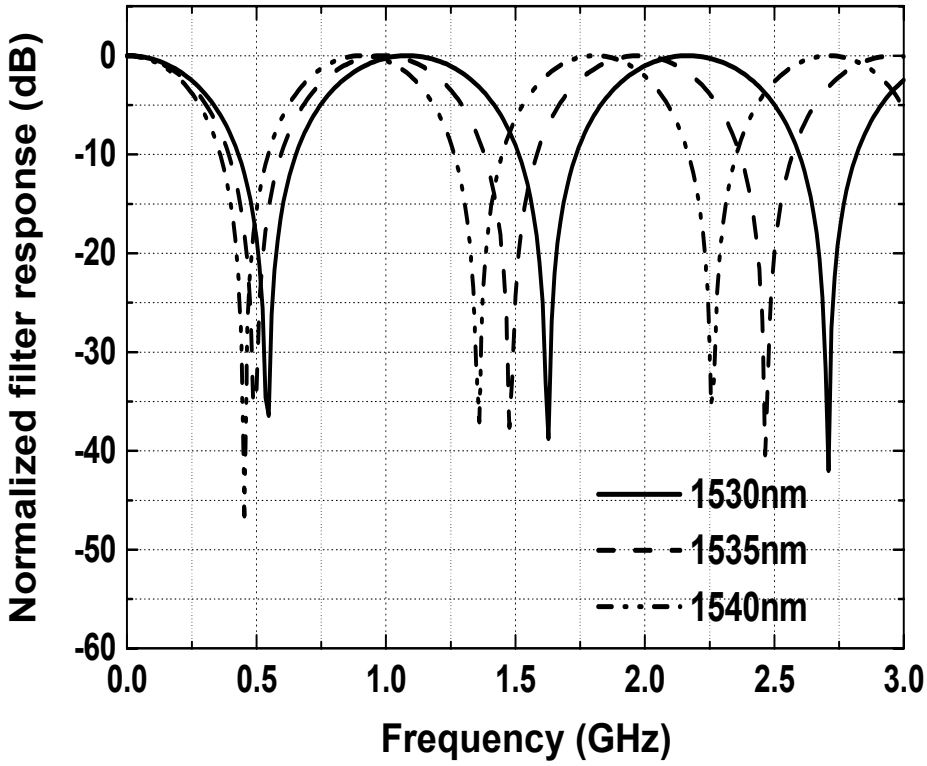

Figure 4.10 Frequency response of the proposed filter.

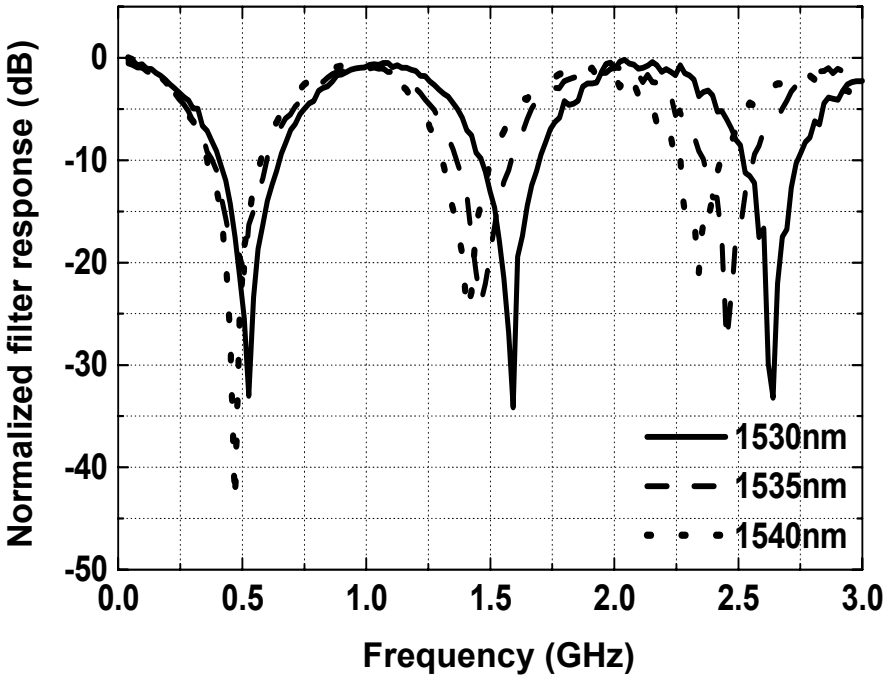

Figure 4.11 Experimental result of frequency response.

Ⅴ. Conclusion

In this thesis, a novel tunable fiber-optic microwave filter having two taps is demonstrated. The time delay line of this filter is produced by velocity difference between two modes, LP_{01} and LP_{02}, guided in DCF, and the weight of tap is controlled by changing the HOF radius which determines the power coupling ratio to be transferred into each mode within DCF from fundamental mode of single mode fiber.

To analyze the filter characteristics, firstly we solved the wave equation in order to obtain the time delay between modes, and then simulated the filter response. And, we measured the filter characteristics. The experimental results did not coincide with the simulation results, because the real structure of DCF and HOF was not same with the design to be considered in simulation. However, we could see the tunable characteristic, which is similar with the simulation results, of the proposed filter according to the source wavelength.

The method to use fiber modes as delay lines has the advantage that optical microwave filter having several taps can be configured with one multi mode fiber and one source. In addition, if the DCF is designed to have more modes, it is possible to make microwave filter having several taps which can be applied to variable applications.

The use of multi mode DCF for generating optical time delay can apply for

variable applications where large bandwidths is needed except microwave filters, such as analog to digital converter [13] or optically controlled phased array antennas, because of compact size and large bandwidth of the fiber.

References

[1] K. Wilner and A. P. van Heuvel, “Fiber-optic delay lines for microwave signal processing,” *IEEE Proc.*, vol. 9, pp. 805, 1976.

[2] K. Jackson, S. Newton, B. Moslehi, M. Tur, C. Cutler, J. Goodman, and H. Shaw, “Optical fiber-delay line signal processing,” *IEEE Microw. Theory Tech.*, vol. 33, no 3, pp. 193-210, 1985.

[3] G. P. Agrawal, *Fiber-Optic Communication Systems*, 1997.

[4] I. Frigyes and A. J. Seeds, “Optically generated true-time delay in phased-array antennas,” *IEEE Trans. Microwave Theory Tech.*, vol. 43, p.2378.

[5] R. Ramaswami and K. N. Sivarajan, *Optical Networks: A Practical Perspective*. 1998

[6] Y. Frankel and D. Ronald, “Fiber-Optic Tunable Microwave Transversal Filter,” *IEEE Photonics Technol. Lett.*, vol. 7, no. 2, pp.191-193, 1995.

[7] D. Norton, S. Johns and R. Soref, “Tunable Microwave Filtering Using High Dispersion Fiber Time Delays,” *IEEE Photonics Technol. Lett.*, vol.6, no. 7, pp. 831-832, 1994.

[8] D.B. Hunter and R.A. Minasian, “Reflectively tapped fiber optic transversal filter using in-fiber Bragg gratings,” *IEE Electron. Lett.*, vol. 31, no.12, pp. 1011-1012, 1995

[9] J. Capmany, D. Pastor, B. Ortega, “New and Flexible Fiber-Optic Delay-line Filters Using Chirped Bragg Gratings and Laser Arrays,” *IEEE Microwave Theory Tech*., vol. 47, no. 7, pp. 1321-1326, 1999.

[10] G. Keisser, *Optical Fiber Communications*, 2000.

[11] D. Gloge, “Weakly guiding fibers,” *Appl. Opt.*, vol.10, pp. 2252-2258, 1971.

[12] S. Choi, W. Shin and K. Oh, “Higher-Order-Mode Dispersion Compensation Technique Based on Mode Converter using Hollow Optical Fiber,” *OFC ’02*(2002), WA6.

[13] F. Coppinger, A.S. Bhushan and B. Jalali, “12Gsamles/s Real-Time Analog-to-Digital Converter Based on Wavelength Division Sampling,” *MWP’99*,

국 문 요 약

광분산 보상 광섬유를 이용한 새로운 구조의 fiber-optic tunable 마이크로파 필터

80년대 이후 광섬유를 이용한 신호처리 방법이 많이 연구되고 있다. 이는 electrical 신호로 처리할 수 없는 수십 GHz이상의 고주파 대역을 optical domain에서 처리할 수 있기 때문이다.

본 논문에서는 optical time delay를 이용하여 새로운 구조의 변조 가능한 마이크로파 필터를 구성하였다. 일반적으로 filter는 delay line과 weight로 이루어진 여러 개의 tap으로 이루어진다. 본 논문에서는 tap 수만큼의 fiber 또는 optical source가 필요한 기존의 방법과 달리, 여러 개의 모드를 가지는 하나의 광섬유를 이용하여 filter를 구성하였다. 새롭게 제시된 이 필터는, 모드간의 time delay를 이용하여 delay line을 구성하였고, 모드간의 파워 비를 조절하여 각 tap의 weight를 조절하였다. 이때, 모드간의 파워 비는 중공 광섬유 (hollow optical fiber)의 중공 반경에 의해 조절된다.

본 논문에서는 새롭게 제시된 이 광 필터의 특성을 simulation과 실험으로 검증하였다. 이를 위해 Maxwell equations으로부터 각 모드간의 time delay를 수치적으로 구하였고, 이를 이용하여 광 필터의 frequency response를 수식으로 표현하였다. 그리고 이 수식으로부터 얻은 결과를 실험과 비교 분석하였다.